Mechanics & Industry **18**, 508 (2017)
© AFM, EDP Sciences 2017
DOI: 10.1051/meca/2017030

Mechanics & Industry

Available online at:
www.mechanics-industry.org

Regular Article

Analysis of the performance of worn hydrodynamic water-lubricated plain journal bearings considering cavitation and elastic deformation

Yanzhen Wang, Zhongwei Yin*, Gengyuan Gao, and Xiuli Zhang

State Key Laboratory of Mechanical System and Vibration, Shanghai Jiao Tong University, Shanghai, PR China

Received: 24 May 2017 / Received in final form: 2 September 2017 / Accepted: 24 September 2017

Abstract. This paper studies the lubrication performance of worn water-lubricated plain journal bearings including effects of cavitation and elastic deformation using computational fluid dynamics (CFD) and fluid–structure interaction (FSI) method, aiming to provide design and analysis references for worn water-lubricated plain journal bearings. The results of the CFD and FSI method of this study are compared with the experimental ones and they are in good agreement. The validated model is used to study the influences of elastic deformation and different wear depth of bush on the performance of water-lubricated journal bearings with different length to diameter ratios. Finally, a method of determining the maximum allowable wear depth of water-lubricated plain journal bearings is proposed. The diagrams of this work could be used to design and analysis of worn plastic water-lubricated plain journal bearings.

Keywords: Worn water-lubricated bearings / computational fluid dynamics / fluid–structure interaction / cavitation

1 Introduction

Water-lubricated journal bearings are widely used in navy ships, boats, pumps and hydroelectric turbines because of their simplicity, efficiency, and low cost [1,2]. The bearings are in mixed and/or boundary lubrication in the start or stop stage and heavy load or low speed operating conditions. During this time, the bearings are prone to wear due to high friction coefficient. To completely understand the behavior of water-lubricated journal bearings in the entire operation period, it is necessary to study the property of bearings with wear pattern.

In recent years, Litwin et al. [3–6], Gertzos et al. [7], and Yin et al. [8–12] have done experimental and theoretical researches on water-lubricated bearings. Litwin [3–6] conducted experimental researches about three layer polymer journal bearings and sintered bronze journal bearings. The results showed that three layer journal bearings ensured minor resistance of movement, good vibration damping property, and easier fitting property. The bronze bearings provided greater load carrying capacity than comparable elastic bearings and could be used in heavy loads with relatively small diameters. Litwin [13] also investigated the influence of local bush wear on load carrying capacity of water-lubricated sliding bearings. The results showed that worn bearings remained fluid lubrication regime and the load carrying capacity increased for the modifications of bush edge shape. Gertzos et al. [7] conducted computational fluid dynamics (CFD) analysis of plain journal bearings lubricated by Bingham lubricant with different performance characteristics, and the results could be helpful for the design of smart journal bearings. Yin et al. [8–12,14] provided references for the designing of water-lubricated plain journal bearings and thrust bearings by CFD method. They also studied the stiffness coefficient and maximum load carrying capacity of misaligned water-lubricated journal bearing in their subsequent research.

For water lubrication, the plastic or rubber bush materials are elastic with low elasticity modulus. Therefore, it is necessary to consider the elastic deformation of bush in analysis. Liu et al. [15] investigated the pressure distribution and center orbit of journal using CFD and fluid–structure interaction (FSI) method and phase change boundary condition. The result showed that the combination of CFD and FSI method was a useful tool for the study of hydrodynamic and elasto-hydrodynamic lubrication and that the elastic deformation of bearings significantly affected the rotor locus. Wang et al. [14] also studied the performance of water-lubricated journal bearing with plastic bush by CFD and FSI method, and a diagram was provided which can be used for the design of composite

* e-mail: merinawang@163.com

journal bearings. Lin et al. [16] proposed a transient analysis method on the lubrication performance of a journal bearing using CFD and FSI technique including both thermal and cavitation effects. Relevant researches also carried out by Shenoy et al. [17]. The approach can be used in predicting bearing performance under dynamic loading conditions. Glavatskih et al. [18] conducted a thermo hydrodynamic (THD) analysis of compliant journal bearings of poly tetra fluoro ethylene material considering liner deformation. The results exhibited that compliant bearings showed increased load carrying capacity, significantly reduced peak pressures and thicker oil film in the loaded zone. However, there are few reports about the lubrication performance of plastic bearings considering shape change caused by wear using CFD and FSI method.

Researches showed that the long time operation of bearing, low rotational speed in the start and stop period, heavy load and misalignment of the shaft are some of the most important factors that produce wear [19]. The wear of plain journal bearings in traditional oil lubrication has attracted attention of many researchers for its importance [20,21]. Dufrane et al. [22] studied worn steam turbine bearings during overhaul periods to determine the extent of wear. And found that significant wear appeared with low turning gear speeds. Two wear geometry models were proposed to analysis the influence of wear on hydrodynamic performance. The model which assumed that the worn arc at a radius larger than the journal was more realistic and was widely used in subsequent research. Hashimoto et al. [23] studied the influence of geometric change due to wear on hydrodynamic lubrication of journal bearing in both laminar and turbulent regimes. The steady state characteristics of journal bearings were analyzed both theoretically and experimentally, and good agreement was obtained. Results showed that the wear of bearing had significant effects on steady-state characteristics. Nikolakopoulos et al. [24] put forward a multi-objective optimization approach for the design of worn or/and misaligned bearings under elasto hydrodynamic conditions. The result provided an engineering tool for the determination of design parameters of plain journal bearings under EHL regimes. Nicodemus et al. [25] studied the influence of wear on the performance of journal bearings under micropolar lubrication using Dufrane's wear model. The results showed that the wear caused by transient start-stop operation had significant effect on bearing performance and it was necessary to consider wear of bearing in analysis. Nicodemus et al. [26] also studied a four-pocket hybrid worn bearing under turbulent regime. Fillon and Bouyer [27,28] investigated the THD performance of a worn plain journal bearing with different wear depth. The results showed that defects up to 20% had little influence whereas above this value (30–50%) the defects created a significant fall in temperature. They also carried out experimental research on a journal bearing subjected to starts and stops, and wear of bearing resulted in an increase in maximum pressure and decrease in temperature.

With the development of computer technology, more and more researches were conducted using CFD and FSI method. CFD and FSI programs provide accurate design for water-lubricated journal bearings, but the process is quite time-consuming. Therefore, this paper studied abundant cases to provide references for the design and analysis of water-lubricated worn plain journal bearings.

To the best of our knowledge, no investigation is yet available in the literatures about the performance of worn water-lubricated journal bearings under EHL operation. Therefore, the present study investigates the lubrication performance of worn water-lubricated journal bearings including effects of elastic deformation and cavitation. The results of the CFD and FSI analysis of water lubrication are compared with the experimental ones of Litwin [29] and they are in good agreement. The performance characteristics of worn plain journal bearing follows the model introduced by Dufrane et al. [22], and the results are found to be in good agreement with the experimental and theoretical work of Hashimoto [23]. The validated model is used to study the influence of bush elastic deformation on the performance of water-lubricated journal bearings. Then the influences of wear depth on bearing performance for different length-to-diameter ratio are investigated. Moreover, according to the results calculated, a method determining the maximum allowable wear depth of water-lubricated plain journal bearings based on wear depth is proposed. The diagrams of this work could be used to design and analysis of worn water-lubricated journal bearings.

2 Numerical analysis

2.1 Governing equations of the fluid domain

The mass and momentum conservation equations are used to predict the performance of fluid domain. The flow is assumed to be incompressible, isoviscous, steady and isothermal, with zero gravitational and other external body force.

$$\nabla\cdot\boldsymbol{\nu} = 0, \tag{1}$$

$$\rho_f\nabla(\boldsymbol{\nu}\cdot\boldsymbol{\nu}) = -\nabla p + \nabla(\tau_f), \tag{2}$$

where ρ_{f} is the fluid density, $\boldsymbol{\nu}$ the fluid velocity vector, p the static pressure and τ_{f} is the stress tensor. The stress tensor can be defined as:

$$\tau_f = \mu_f[(\nabla\boldsymbol{\nu} + \nabla\boldsymbol{\nu}^T) - 2/3\nabla \times \boldsymbol{\nu}I], \tag{3}$$

where μ_{f} is the fluid viscosity and I is the unit tensor.

The load carrying capacity can be calculated by integrating the pressure over the journal surface as follows:

$$F_x = \int_0^L \int_0^{2\pi} p\cos\theta R_j d\theta dz, \tag{4}$$

$$F_y = \int_0^L \int_0^{2\pi} p\,sin\,\theta R_j d\theta dz. \tag{5}$$

Table 1. Parameters of the models.

Parameters	Value
Bearing diameter	80 mm
Length to diameter ratio	0.5, 1, 1.5
Eccentricity	0.1, 0.2, 0.3, 0.4, 0.5, 0.6, 0.7, 0.8, 0.9, 0.95
Angular velocity	314.16 rad/s
Saturation water vapor pressure	2340 Pa
Saturation density of water	998.2 kg/m^3
Saturation density of water vapor	0.5542 kg/m^3
Dynamic viscosity of water	0.001 Pa·s
Dynamic viscosity of water vapor	1.34E−5 Pa·s
Elastic modulus of bearing	1300 MPa
Poisson's ratio of bearing	0.44
The compressive stress at strain value of 1.0 of bearing	1.94 MPa

2.2 Fluid–structure interaction

The solid domain follows the second law of motion, which can be described as follows:

$$\rho_s \ddot{\mathbf{d}}_s = \nabla\cdot\boldsymbol{\sigma}_s + \mathbf{f}_s, \tag{6}$$

where ρ_s is the solid density, $\mathbf{d}_s$ the local acceleration of the solid domain, $\boldsymbol{\sigma}_s$ the solid stress tensor and $\mathbf{f}_s$ is the body force vector.

The fluid and structure interact with each other for the fluid pressure makes the bearing deformation. In turn, the deformation of bearing changes the shape of the fluid domain. The nodes on the fluid–solid interface correspond to the displacement compatibility and traction equilibrium equations.

$$\begin{cases} \mathbf{d}_f = \mathbf{d}_s \\ \mathbf{n}\cdot\boldsymbol{\tau}_f = \mathbf{n}\cdot\boldsymbol{\tau}_s \end{cases}, \tag{7}$$

where $\mathbf{d}_\mathrm{f}$ and $\boldsymbol{\tau}_\mathrm{f}$ are the displacement and stress of fluid domain, respectively, and $\mathbf{d}_\mathrm{s}$ and $\boldsymbol{\tau}_\mathrm{s}$ are the structure displacement and stress, respectively.

In this study, the equations are solved by direct computing approach. The governing equations for the fluid and solid domain are combined in one matrix system:

$$\begin{bmatrix} \mathbf{A}_\mathrm{ff} & \mathbf{A}_\mathrm{fs} \\ \mathbf{A}_\mathrm{sf} & \mathbf{A}_\mathrm{ss} \end{bmatrix} \begin{bmatrix} \Delta \boldsymbol{X}_\mathrm{f}^k \\ \Delta \boldsymbol{X}_\mathrm{s}^k \end{bmatrix} = \begin{bmatrix} \boldsymbol{F}_\mathrm{f} \\ \boldsymbol{F}_\mathrm{s} \end{bmatrix}, \tag{8}$$

where $\mathbf{A}_\mathrm{ff}$, $\mathbf{A}_\mathrm{ss}$, $\mathbf{A}_\mathrm{fs}$, $\mathbf{A}_\mathrm{sf}$ are the system matrix for fluid, solid and the coupling effects respectively. $\Delta \boldsymbol{X}_\mathrm{f}^k$, $\Delta \boldsymbol{X}_\mathrm{s}^k$ are the solution for fluid and solid domain respectively. $\boldsymbol{F}_\mathrm{f}$ and $\boldsymbol{F}_\mathrm{s}$ are the external force for fluid and solid domain respectively. And k is the iteration number. Thermal effect is not considered in this study for they have little influence on water in open environment.

2.3 Cavitation model

For water-lubricated journal bearings, cavitation has significant influence on lubrication performance. When flow enters the divergence domain, water film pressure might fall below the saturation water vapor pressure, and the water film would rupture and cavitation occurs. Thus cavitation is taken into account in calculations. The liquid–vapor mass transfer (evaporation and condensation) is governed by the following equation:

$$R_b \frac{\mathrm{d}^2 R_b}{\mathrm{d}t^2} + \frac{3}{2}\left(\frac{\mathrm{d}R_\mathrm{b}}{\mathrm{d}t}\right)^2 + \frac{2\sigma}{\rho_\mathrm{f} R_\mathrm{b}} = \frac{p_\mathrm{g} - p}{\rho_\mathrm{f}}, \tag{9}$$

where R_b is the bubble radius, p_g the pressure in the bubble and σ is the surface tension coefficient between the liquid and vapor. Neglecting the second order terms (which is appropriate for low oscillation frequencies) and the surface tension, this equation reduces to:

$$\frac{\mathrm{d}R_\mathrm{b}}{\mathrm{d}t} = \sqrt{\frac{2}{3}\frac{p_v - p}{p_f}}. \tag{10}$$

Then the total interphase mass transfer rate per unit volume is

$$\dddot{m}_\mathrm{fg} = F\frac{3r_\mathrm{nuc}(1 - r_g)\rho_g}{R_\mathrm{nuc}}\sqrt{\frac{2}{3}\frac{|p_v - p|}{p_f}} sgn(p_v - p), \tag{11}$$

where R_nuc is the nucleation site radius, r_g the volume fraction of bubble, ρ_g the vapor density and r_nuc is the volume fraction of the nucleation sites. In equation (11), $\mathrm{sgn}(p_\mathrm{v} - p)$ is the symbolic function.

$$sgn(p_v - p) = \begin{cases} 1, & p_\mathrm{v} - p > 0 \\ 0, & p_\mathrm{v} - p = 0 \\ -1, & p_\mathrm{v} - p < 0 \end{cases}. \tag{12}$$

The Rayleigh–Plesset cavitation model implemented in CFX adopts the following defaults for the model parameters: $R_\mathrm{nuc} = 10^{-6}$ m, $r_\mathrm{nuc} = 5 \times 10^{-4}$, $F_\mathrm{vap} = 50$, $F_\mathrm{cond} = 0.01$.

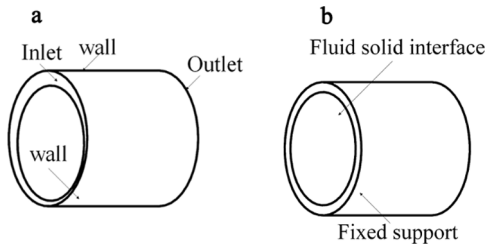

Fig. 1. Boundary conditions of fluid domain and solid domain.

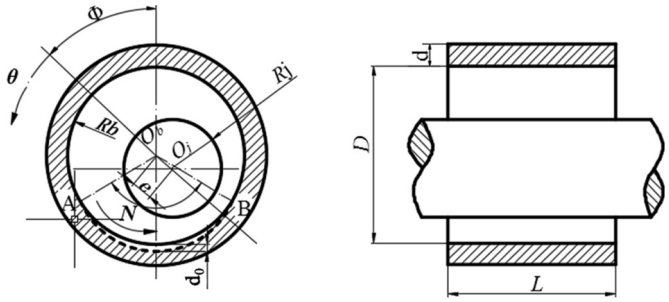

Fig. 2. Worn plain journal bearing model.

2.4 Solution method

The solution method of this study was similar to Wang et al. [14]. The bearing was submersed in water, and the water properties were considered to be constant in the simulation. The diameter of the bearing was 80 mm, the bearing clearance was 0.15%, and the angular velocity of journal was 314.16 rad/s. According to the size and the speed of the journal, the Reynolds number $\left(Re = \frac{\rho_f NRC}{\mu_f} = 753.6\right)$ in the present study was lower than the critical Reynolds number ($Re_c = 2000$), thus the fluid flow was assumed to be laminar. The operation pressure was set to 101 325 Pa due to the fact that the stern bearings were immersed in water in operation and that the pressure of inlet and outlet was approximately equal to atmospheric pressure. Table 1 lists the corresponding parameters. The bearing material was 12.5 wt.% glass fiber and 12.5 wt.% carbon fiber filled ultrahigh molecular weight polyethylene (UHMWPE), and the elastic modulus was 1300 MPa and the Poisson's ratio was 0.44 according to experiment results. Besides, the compressive stress at strain value of 1.0 of bearing material is 1.94 MPa.

The water film model was meshed in Gambit 2.4 using hexahedral grids. The boundary conditions of the fluid domain were shown in Figure 1a, where two end faces of the water film were set as inlet and outlet with film pressure equaling to ambient pressure, outer face of the water film was modeled as "stationary wall", and the inner face was set as "moving wall" with a rotational speed equaling the angular velocity of the shaft. The sensitivity of mesh density to load carrying capacity was checked both for the fluid and solid domain. The mesh distributions in the axial, circumferential and radial directions were $50 \times 100 \times 6$ for the solid domain. For fluid domain, there were 12 divisions in the radial direction and 300 divisions in the circumferential direction. The mesh density in the axial direction was 40 cells for $L/D = 0.5$, 80 cells for $L/D = 1$, and 120 cells for $L/D = 1.5$.

The structure model of bearings was created in ANSYS Workbench. The bearing was considered to be elastic and shaft was considered to be rigid. The boundary conditions of the bearing were shown in Figure 1b, where the outside and inside surface of the bearing were set as fixed support and fluid solid interface, respectively.

The numerical results were calculated by CFD package ANSYS CFX. As previously stated, cavitation was modeled using Rayleigh–Plesset model. The time step was set to 0.002 s in the simulation. The convergence of the computing method was set as high resolution. The minimum and maximum iteration steps of convergent control were set as 1 and 100 respectively. The minimum and maximum iteration steps of coupling step control were 1 and 10 respectively. Results were deemed acceptable if the difference was <1E−5.

3 Models

3.1 Worn plain journal bearing model

In the present study, the geometry of the worn water-lubricated journal bearing follows the model described by Dufrane et al. [22]. Reference [22] proposed two wear models to analyze the influence of wear on hydrodynamic lubrication, one based on the concept that imprint the journal in the bearing, and the other one based on a hypothesis that the radius of worn arc is larger than the shaft. The experimental results showed that the model with worn arc at a radius larger than the shaft was more accurate, so this model was used in the present study. Figure 2 shows the schematic of worn journal bearing, where R_j and R_b are the radius of journal and bearing respectively, and e is the distance between the center of journal (O_j) and the center of bearing (O_b). The radial clearance (C) is defined as the difference between R_j and R_b, and the eccentricity ratio (ε) is the ratio between e and C. Dufrane et al. [22] proposed that the wear pattern was located almost exactly symmetrically at the bottom of the bearing, and the width was uniform along the length of bearing. The model can be described by the following the equation:

$$\frac{d'}{C} = \frac{d_0}{C} - (1 + \cos\theta), \tag{13}$$

$$\delta = \frac{d_0}{C}. \tag{14}$$

where θ is the bearing angle, d' the wear depth at angle of θ, d_0 the maximum wear depth and δ is the maximum dimensionless wear depth.

The maximum wear depth is 50% of the bearing radial clearance. The change in bearing geometry is given by equation (15)

$$\delta h = d' = d_0 - C - C\cos(\theta). \tag{15}$$

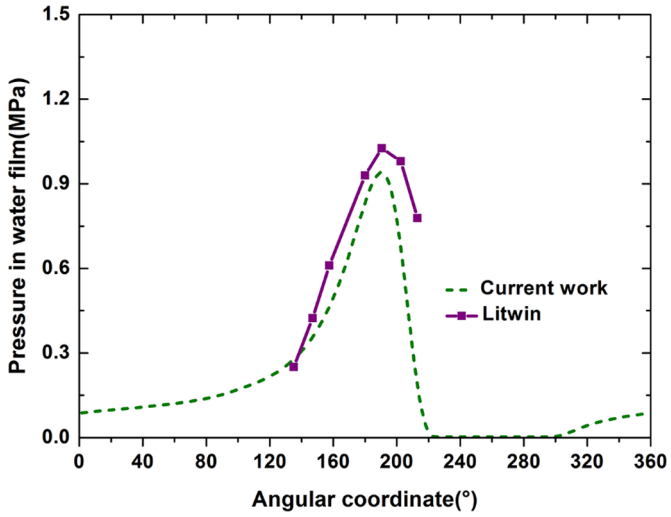

Fig. 3. Comparison of pressure distribution with reference [29].

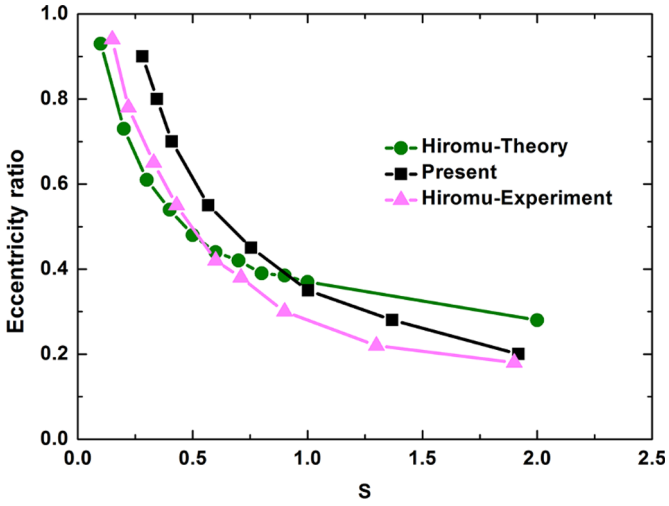

Fig. 4. Comparison of variation of eccentricity ratio vs. Sommerfeld number with results in reference [23] for $\delta = 0.5$ and $Re = 137$.

The maximum dimensionless wear depth ($\delta = d_0/\mathrm{C}$) which corresponds to the ratio of the wear depth and the radial clearance is used in the calculation. Besides, the value of wear depth is given in equation (16), which is added in the calculation of water film thickness.

$$\begin{cases} \delta\mathrm{h} = \mathrm{C}[\delta - 1 - \cos(\theta)] & \text{for } \theta_\mathrm{A} \leq \theta \leq \theta_\mathrm{B} \\ \delta\mathrm{h} = 0 & \text{for } \theta < \theta_\mathrm{A} \text{or} \theta > \theta_\mathrm{B} \end{cases}, \tag{16}$$

As shown in Figure 2, the angles θ_A and θ_B are the beginning and the end of the wear region, which are calculated from the equation: $\cos(\theta) = \delta - 1$.

For the case of a worn water-lubricated journal bearing, the film thickness follows equation (17).

$$\mathrm{h} = C + \mathrm{e}\cos(\theta) + \delta\mathrm{h}. \tag{17}$$

3.2 Validation of the model

The CFD algorithm used had been validated by experiments study in our previous studies [8]. The experimental results showed that the eccentricity ratio was in the range of 0.55–0.65 when the calculated eccentricity ratio was 0.6 under the same work condition. The calculated results were in well agreement with the experimental one. Besides, the pressure distribution and eccentricity ratio vs. Sommerfeld number calculated in this work were compared with literatures for further validation. In the present study, the Sommerfeld number S was given by:

$$\mathrm{S} = \frac{\mu_\mathrm{f}\mathrm{NDL}}{\mathrm{F}}\left(\frac{\mathrm{R}}{\mathrm{C}}\right)^2. \tag{18}$$

In Figure 3, the pressure distribution of the water film in this work by CFD model was compared with the experimental results of elastic bearings in reference [29]. The operation parameters in Figure 3 were: bearing diameter 100 mm, bearing length 150 mm, radial clearance 75 μm, rotational speed 660 rpm, and specific pressure 0.2 MPa. Figure 3 showed that the results in this work agreed well with the experimental results of reference [29]. The maximum percentage difference of the present method and the experimental results was 8.3%, which might be caused by the difference in elasticity modulus of bush materials and the imperfect shape of the test bush.

In Figure 4, the relationship of eccentricity ratio vs. Sommerfeld number were compared with the measured and theoretical results in reference [23] with the parameter of $\delta = 0.5$ and $\mathrm{Re} = 137$. And the Reynolds number Re was given by equation (19). Figure 4 showed that the results in this work were consistent with the experimental and theoretical results in reference [23]. Reference [23] did not take the variation of viscosity of oil with temperature into account, which leads to the load carrying capacity higher than actual value. Besides, the calculation methods and the models used in reference [23] and the present study were different. These might be the reasons for the difference between this paper and reference [23].

$$\mathrm{Re} = \frac{\rho_\mathrm{f} NRC}{\mu_\mathrm{f}}. \tag{19}$$

4 Results and discussion

Figure 5 presents the hydrodynamic water film pressure under different boundary conditions and film thickness distribution at the mid-plane with $D = 80\mathrm{mm}$, $L/D = 1$, $\psi = 0.15\%$, $N = 314.16\,\mathrm{rad/s}$, and $\varepsilon = 0.8$. Cavitation occurs when water film pressure lower than the saturation vapor pressure of water [9]. And cavitation plays a more important role in water lubrication than oil lubrication for the saturation vapor pressure of water is much higher than oil. It can be observed from Figure 5a that the pressure distribution of water film without consideration of cavitation presents great negative pressure. Actually, the water film cannot bear negative pressure and it ruptured when the pressure lower than 2340 Pa. Meanwhile, the maximum film pressure without consideration of cavitation

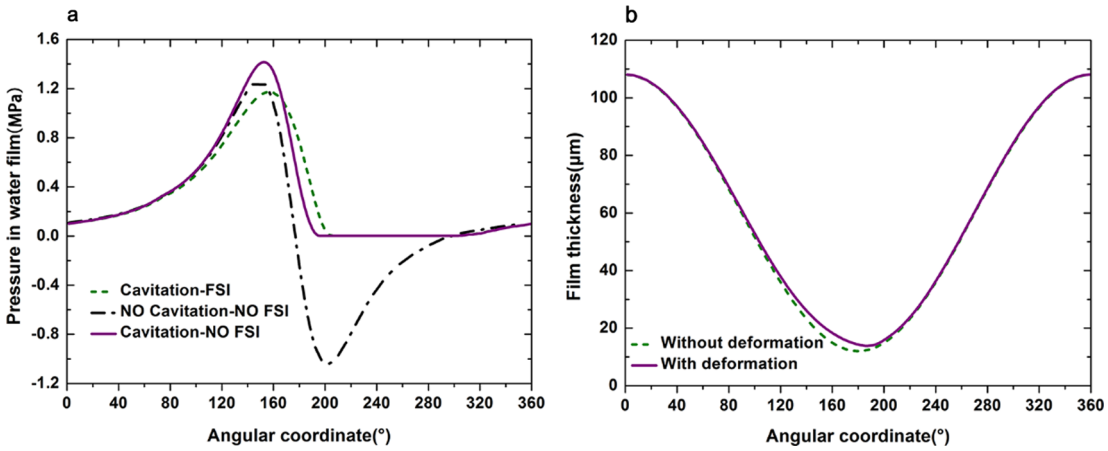

Fig. 5. The pressure and film thickness distribution of water film for different boundary conditions.

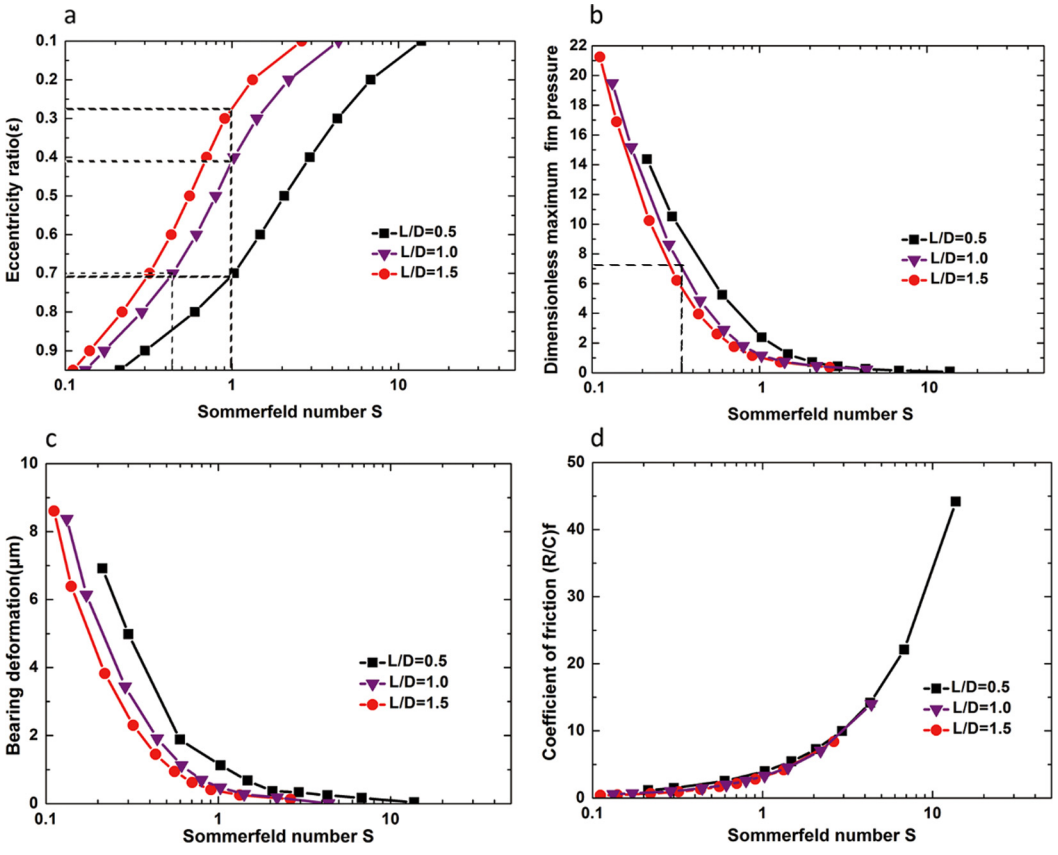

Fig. 6. Eccentricity ratio, maximum film pressure, bearing deformation, and coefficient of friction vs. Sommerfeld number for elastic bearing with bush thickness of $d = 10$ mm.

is 10.75 % lower than the result considering cavitation. Thus it is necessary to include the influence of cavitation in simulations to accurate describe the pressure distribution of water film.The bush has significant deformation with the increase of load for the bush material is plastic and the elastic modulus is only 1300 MPa. As shown in Figure 5a, the maximum pressure with consideration of elastic deformation is 17.11% lower than the rigid bush. Besides, the circumferential angle of maximum pressure increased 4.4 and the distribution of pressure are smoother compared with rigid bearing. Therefore, it is necessary to include the deformation of bush in simulation for plastic water-lubricated journal bearings.

Figure 5b presents the comparison of film thickness distribution in the mid-plane of elastic bush and rigid one. In the convergence region of water film, the film thickness of elastic bush is larger than the rigid one. In the divergency region of water film, the film thickness of elastic bush and rigid bush are almost coinciding. For plastic journal bearings, the water film thickness in the convergence region

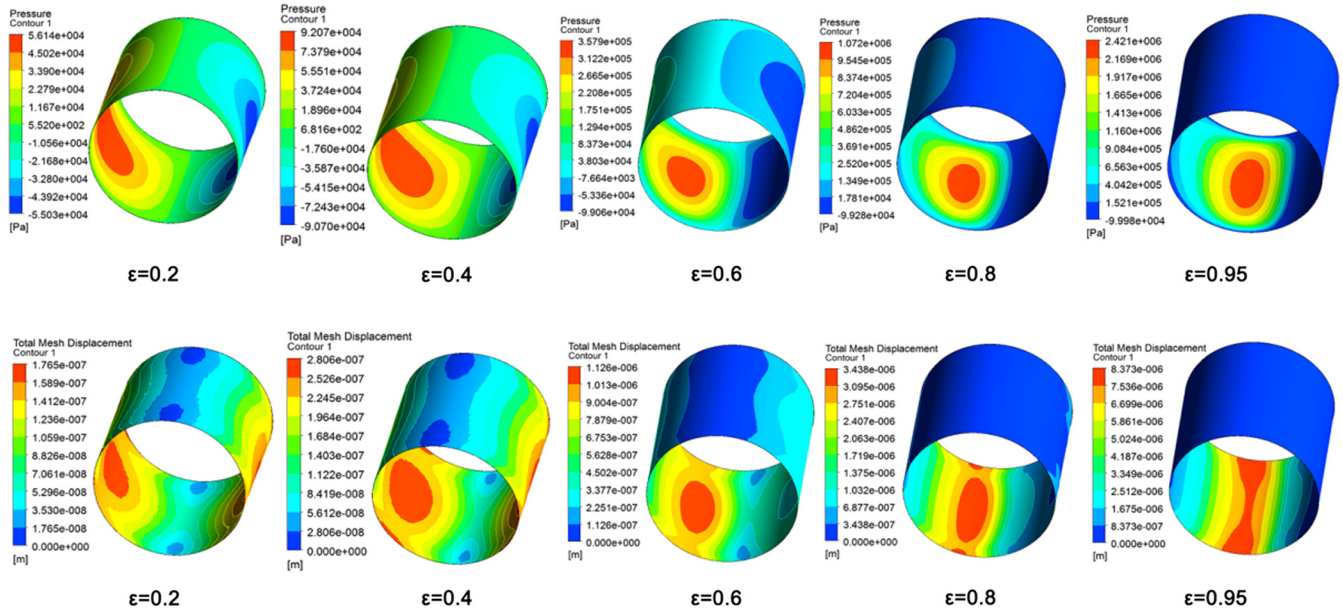

Fig. 7. Contours of static pressure (Pa) and deformation (μm) for different eccentricity ratio.

increased for the deformation of bush, and the minimum film thickness increased 15.38%. Thus the load carrying capacity decreased in consequence for the increase in water film thickness.

Figure 6 presents the relationship of eccentricity ratio, maximum film pressure, bearing deformation, and coefficient of friction vs. Sommerfeld number for elastic bush with L/D equals to 0.5, 1.0, and 1.5. Among them, X-axis is the log S, and Y-axis is the eccentricity ratio ε, dimensionless maximum film pressure, maximum bearing deformation, and dimensionless friction coefficient, respectively. Other parameters are: $D = 80$ mm, $d = 10$ mm, $\psi = 0.15\%$, $\varepsilon = 0.1$–0.95, and $N = 314.16$ rad/s.

As shown in Figure 6a, the eccentricity ratio decreases with an increase in Sommerfeld number. The curvature of the curve varies with the increase of Sommerfeld number. The relationship between $\log S$ and eccentricity ratio is basically linear when the eccentricity ratio is between 0.4–0.7, and the slope decreases when the eccentricity is less than 0.3 or greater than 0.7. Sommerfeld number increases with a decrease in L/D for a constant eccentricity ratio ε, and the smaller the value of L/D, the more Sommerfeld number increases. This shows that the side leakage of bearing increase with a decrease of L/D value, which accelerates the reduction of load carrying capacity.

For plastic water-lubricated journal bearings, the eccentricity ratio can be determined by Figure 6a when Sommerfeld number is calculated for different L/D values before design of bearings. When the value of eccentricity ratio is known, the minimum water film thickness and the lubrication regimes of bearings can be determined, which can be used as a reference for design of plastic water-lubricated plain journal bearings. For example, the value of eccentricity ratio is 0.71, 0.41, 0.28 when L/D equals to 0.5, 1.0, 1.5 for Sommerfeld number equals to 1.0, respectively. Then the value of minimum water film thickness can be determined by equation (20) and the lubrication regimes can also be determined by the calculation of film thickness ratio parameter defined as equation (21) [30].

$$h_{min} = C(1 - \varepsilon). \tag{20}$$

$$\lambda = \frac{h_{min}}{\eta} = \frac{h_{min}}{\sqrt{\eta_1^2 + \eta_2^2}}, \tag{21}$$

where λ is the film thickness ratio, η is the combined surface roughness, η_1 and η_2 are the roughness height of the bearing and shaft surfaces. Generally, the lubrication regimes can be determined as follows: $\lambda \geq 3$ for hydrodynamic lubrication or elastic hydrodynamic lubrication regime, $1 \leq \lambda \leq 3$ for mixed lubrication states and $0 < \lambda < 1$ for boundary lubrication states.

The results in Figure 6b–d can be used to determine the operation parameters of plastic water-lubricated journal bearings. Figure 6b shows the relationship between dimensionless maximum film pressure $\left(P = P_{\max}\frac{\psi^2}{\mu N}\right)$ and Sommerfeld number. As shown in Figure 6b, the dimensionless maximum film pressure decreases with an increase in Sommerfeld number, and the slope of the curve decreases significantly and the maximum film pressure finally falls to the same value for different L/D ratio. And for a constant Sommerfeld number, the value of maximum film pressure increases as the decrease of L/D. Figure 6c shows the relationship between maximum bush deformation and Sommerfeld number. As shown in Figure 6c, the maximum deformation of bearing also decreases as the increase of Sommerfeld number. For a constant Sommerfeld number, the value of maximum deformation increases as the decrease of L/D. Figure 6d shows the relationship between dimensionless friction coefficient and Sommerfeld number. As shown in Figure 6d, the dimensionless friction coefficient increases significantly with the increase of

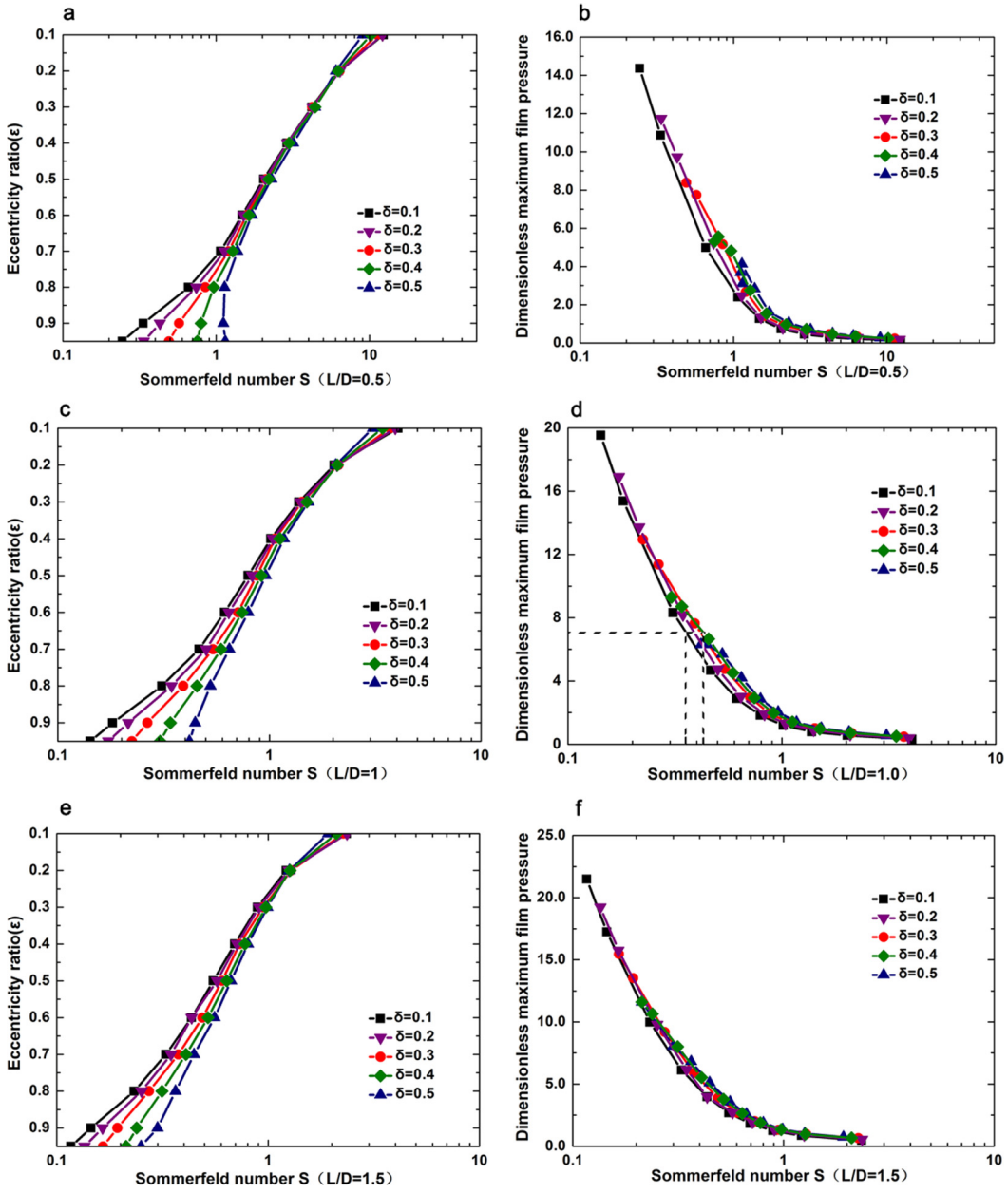

Fig. 8. The eccentricity ratio and dimensionless maximum film pressure vs. Sommerfeld number for different wear depth.

Sommerfeld number. The thickness of water film increases with the increase of Sommerfeld number, so the viscous shearing force between liquid molecules increase, which results in the increase of friction coefficient.

For plastic water-lubricated journal bearings, the lubrication parameters can be determined by Figure 6 with the calculation of Sommerfeld number for different L/D values. For example, for $S=1.0$ and $L/D=1.0$, the value of maximum film pressure, maximum bush deformation and friction coefficient is 1.6, 0.5 and 3.0 respectively. The lubrication states and the operation parameters can be determined by the conclusion of Figure 6, and the results can be used as references for the design of water-lubricated elastic journal bearings.

Figure 7 shows the contours of static pressure (Pa) and deformation (μm) for $\varepsilon=0.2$–0.95, $N=314.16$ rad/s, $\psi=0.15\%$. As the increase of eccentricity ratio, the maximum film pressure increases, while the bearing areas of pressure decrease. The bearing tends to produce stress concentration under the double role of increase in pressure and decrease in bearing area. Figure 7 also shows the contours of displacement of interface under different eccentricity ratio. The displacement distributions and pressure distributions are inconsistent at high eccentricity ratio due to the boundary condition of two end faces of bearing is free, and it exists displacement in Z direction (axial direction). The results also show that the deformation of bush increase while the deformation regions

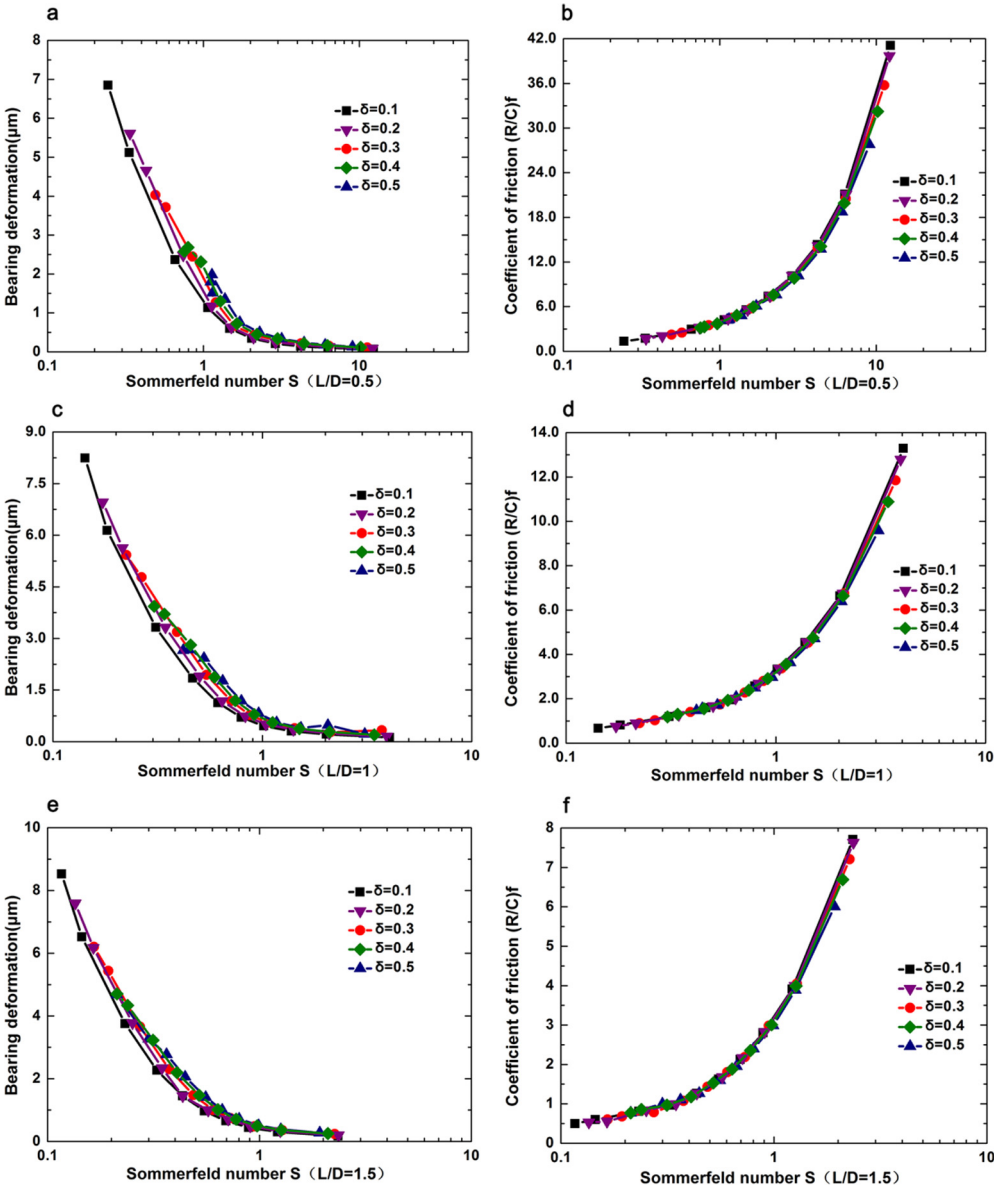

Fig. 9. The maximum bearing deformation and coefficient of friction vs. Sommerfeld number for different wear depth.

decrease as the increase of eccentricity ratio. Therefore, it should avoid excessive load in the operation of bearings to avoid stress concentration of bearing material.

Hereinbefore, the lubrication performance of bearing without wear has been calculated, which can be used as a comparison of worn bearings. In case of heavy or frequent start and stop situations, it is easy to cause wear of bearings and the performance of bearings has significant change after wear. Therefore, the lubrication performance of worn bearings is elaborated in detail to provide reference for the prediction of performance of water-lubricated plain journal bearings.

Figure 8 shows the eccentricity ratio and dimensionless maximum film pressure vs. Sommerfeld number for different wear depth. The parameters are: $d = 10$ mm, $\psi = 0.15\%$, $L/D = 0.5$, 1.0, 1.5, $\delta = 0.1$–0.5, $\varepsilon = 0.1$–0.95, and $N = 314.16$ rad/s. As shown in Figure 8a, c, and e, the eccentricity ratio at the same Sommerfeld number increases as the increase of wear depth, indicating that the load carrying capacity decrease as the increase of wear depth, and this tendency is more pronounced as the decrease of Sommerfeld number and L/D ratio. Moreover, the effects of wear depth on the maximum film pressure are not strong at large Sommerfeld number, but the effects become significant as the decrease of Sommerfeld number. The maximum film pressure increases with an increase in wear depth when Sommerfeld number is higher than 0.8, which indicates that the stress concentration of bearing material will be serious with increase in wear depth. As the decrease of L/D ratio, the influence of wear depth on maximum film pressure becomes strong for a constant Sommerfeld number. This indicates that the maximum film pressure increase more for low L/D ratio after wear, that is, short bearing is more likely to fail for the effect of wear is more significant.

Figure 9 shows the maximum bearing deformation and dimensionless coefficient of friction vs. Sommerfeld number for different wear depth with $d = 10\,\text{mm}$, $\psi = 0.15\%$, $L/D = 0.5$, 1.0, 1.5, $\delta = 0.1$–0.5, $\varepsilon = 0.1$–0.95, and $N = 314.16\,\text{rad/s}$. The results showed that the maximum bearing deformation increases after wear. And the influence of wear depth on bearing deformation becomes weak as the increase of Sommerfeld number and L/D ratio. The friction coefficient of bearings decreases after wear. Besides, the friction coefficient of bearings with different wear depth increases with Sommerfeld number because the thickness of water film increase with the increase of Sommerfeld number, thus the viscosity effect increase and is needs greater force to shear the fluid.

The diagrams of Figures 8 and 9 can be used to evaluate the load carrying properties and lubrication properties of worn water-lubricated plain journal bearings. The conclusions can be used to judge whether the wear depth exceeds the allowable range. We propose that the bearings can no longer be used when the maximum film pressure exceeds 30% of σ_1 of bush material, because the maximum film pressure and maximum deformation of bearing increase significantly when the maximum film pressure exceeds 30% of σ_1. For GF/CF/UHMWPE bush in the present study, the value of σ_1 is 1.94 MPa measured by compressive property experiments. For the intact bearing at $L/D = 1$, the dimensionless film pressure value is 7.2 (as shown in Fig. 6) when the film pressure is 30% of σ_1. Therefore, the allowable maximum dimensionless film pressure for the worn bearings is given by the value of 7.2, too. If the decrease of load carrying capacity for different wear depth is not exceeding 20% when the dimensionless maximum film pressure is 7.2, the bearing can continue to use. Otherwise, the bearing cannot continue to use. It is considered that 20% decrease in load carrying capacity is significant, and the bearings no longer suitable for use at this point. As an example (in the case of $L/D = 1$), the Sommerfeld number is 0.32 (Fig. 6b) when the maximum film pressure (when the dimensionless film pressure is 7.2) is 30% of σ_1 for the intact bearing, the Sommerfeld number 0.34 (Fig. 8d) for wear depth being 0.1, and Sommerfeld number is 0.41 (Fig. 8d) for wear depth being 0.4. Thus the decrease in load carrying capacity is 28.12% when wear depth is 0.4 and it exceeds the value of 20%, therefore, the value of wear depth of 0.4 is too large to accept. In other words, the bearing cannot continue to use when wear depth higher than 0.4. Other cases can be judged with the similar method.

Therefore, this paper proposes a reference for the allowable wear depth of water-lubricated plain journal bearings. The wear of bearing and bearing lifetime is closely related due to excessive increase in water film pressure and bush deformation. It will result in stress concentration and further fatigue wear of bush material if continue to use. According to the diagrams calculated, if the decrease in load carrying capacity exceeds 20% at the allowable maximum film pressure, we propose that the bearing is not suitable for further use. And the wear depth at this time is the maximum allowable wear depth.

5 Conclusions

The tribological performance of worn water-lubricated plain journal bearings in hydrodynamic lubrication were examined numerically using CFD and FSI method. Cavitation of water and deformation of bush were taken into account in the simulation. The model used was validated firstly, and the influences of bush elastic deformation, wear depth, length-to-diameter ratio on the performance of water-lubricated journal bearings were studied. The diagrams were presented in the dimensionless form which can be easily used in the design and analysis of water-lubricated worn journal bearings. The following conclusion can be drawn:

- Cavitation and elastic deformation have significant influence on performance of plastic water-lubricated plain journal bearings. The negative pressure is eliminated in divergency region and the maximum film pressure increased when taking into account of cavitation of water. The maximum film pressure decrease and the distribution of pressure is smoother when taking into account elastic deformation, which can be attribute to the increased water film thickness. Therefore, it is necessary to consider the influence of cavitation and elastic deformation for water-lubricated bearings in simulation.
- For worn water-lubricated plain journal bearings, the maximum film pressure and the maximum bearing deformation increase with an increase in wear depth under the same Sommerfeld number. Moreover, the increase in film pressure and bearing deformation results in stress concentration of bearing material, which will accelerate the damage of bush material.
- The dimensionless friction coefficient decreases as the increase of wear depth under the same Sommerfeld number.
- According to the diagrams calculated, if the decrease in load carrying capacity exceeds 20% at the allowable maximum film pressure, we propose that the bearing is not suitable for further use. And the wear depth at this time is the maximum allowable wear depth.

Nomenclature

ρ_f	fluid density
$\boldsymbol{v}$	fluid velocity vector
p	static pressure
τ_f	stress tensor of the fluid region
μ_f	fluid viscosity
I	unit tensor
ρ_s	solid density
$\mathbf{d}_s$	local acceleration of the solid domain
$\boldsymbol{\sigma}_\text{s}$	solid stress tensor
$\mathbf{f}_\text{s}$	body force vector
$\mathbf{d}_\text{f}$	fluid displacement
$\mathbf{d}_\text{s}$	structure displacement
$\boldsymbol{\tau}_\text{s}$	structure stress
$\mathbf{A}$	system matrix

$\Delta \boldsymbol{X}$	solution
$\boldsymbol{F}_{\mathrm{f}}$	external force for fluid domain
$\boldsymbol{F}_{\mathrm{s}}$	external force for solid domain
k	iteration number
R_{b}	bubble radius
p_{g}	pressure in the bubble
σ	surface tension coefficient between the liquid and vapor
R_{nuc}	nucleation site radius
r_{g}	volume fraction of bubble
ρ_{g}	vapor density
r_{nuc}	volume fraction of the nucleation sites
θ	the bearing angle
d_0	the maximum wear depth
d'	the wear depth at angle of θ
δ	the maximum dimensionless wear depth ($\delta = d_0/C$)
δh	the change in bearing geometry due to wear
C	radial clearance
ψ	relative clearance ($\psi = C/R$)
ε	eccentricity
D	the diameter of the bearing
L	the length of the bearing
d	the thickness of the polymer bush
F	the load carrying capacity of bearing
N	the angular velocity of bearing
R	the radius of journal
S	Sommerfeld number $\left(S = \frac{\mu_f NDL}{F}\left(\frac{R}{C}\right)^2\right)$
Re	Reynolds number $\left(Re = \frac{\rho_{\mathrm{f}} NRC}{\mu_{\mathrm{f}}}\right)$
λ	the film thickness ratio
η	the combined surface roughness
η_1, η_2	roughness height of the bearing and shaft surfaces
σ_1	the compressive stress at strain value of 1.0
$t_{\max}$	the maximum bush deformation
$h_{\min}$	the minimum film thickness
$P_{\max}$	the maximum film pressure
P	the dimensionless maximum film pressure $\left(P = P_{\max}\frac{\psi^2}{\mu N}\right)$

References

[1] R. Pai, D.J. Hargreaves, Water Lubricated Bearings, Springer, Berlin, Heidelberg, 2012, pp. 347–391

[2] R. Pai, D.J. Hargreaves, Water lubricated bearings, in: M. Nosonovsky, B. (ed.), Green Tribology, Springer, Berlin, Heidelberg, 2012, pp. 347–391

[3] W. Litwin, Influence of main design parameters of ship propeller shaft water-lubricated bearings on their properties, Pol. Marit. Res. 17 (2010) 39–45

[4] W. Litwin, Experimental research on water lubricated three layer sliding bearing with lubrication grooves in the upper part of the bush and its comparison with a rubber bearing, Tribol. Int. 82 (2015) 153–161

[5] W. Litwin, Properties comparison of rubber and three layer PTFE-NBR-bronze water lubricated bearings with lubricating grooves along entire bush circumference based on experimental tests, Tribol. Int. 90 (2015) 404–411

[6] W. Litwin, A. Olszewski, Water-lubricated sintered bronze journal bearings—theoretical and experimental research, Tribol. Trans. 57 (2013) 114–122

[7] KP. Gertzos, PG. Nikolakopoulos, CA. Papadopoulos, CFD analysis of journal bearing hydrodynamic lubrication by Bingham lubricant, Tribol. Int. 41 (2008) 1190–1204

[8] G. Gao, Z. Yin, D. Jiang, X. Zhang, Numerical analysis of plain journal bearing under hydrodynamic lubrication by water, Tribol. Int. 75 (2014) 31–38

[9] G. Gao, Z. Yin, D. Jiang, X. Zhang, Y. Wang, Analysis on design parameters of water-lubricated journal bearings under hydrodynamic lubrication, Proc. Inst. Mech. Eng. J: J. Eng. Tribol. 230 (2015) 1019–1029

[10] X. Zhang, Z. Yin, G. Gao, Z. Li, Determination of stiffness coefficients of hydrodynamic water-lubricated plain journal bearings, Tribol. Int. 85 (2015) 37–47

[11] X. Zhang, Z. Yin, D. Jiang, G. Gao, The design of hydrodynamic water-lubricated step thrust bearings using CFD method, Mech. Ind. 15 (2014) 197–206

[12] X. Zhang, Z. Yin, D. Jiang, G. Gao, Y. Wang, X. Wang, Load carrying capacity of misaligned hydrodynamic water-lubricated plain journal bearings with rigid bush materials, Tribol. Int. 99 (2016) 1–13

[13] W. Litwin, Influence of local bush wear on water lubricated sliding bearing load carrying capacity, Tribol. Int. 103 (2016) 352–358

[14] Y. Wang, Z. Yin, D. Jiang, G. Gao, X. Zhang, Study of the lubrication performance of water-lubricated journal bearings with CFD and FSI method, Ind. Lubr. Tribol. 3 (2016) 341–348

[15] H. Liu, H. Xu, PJ. Ellison, Z. Jin, Application of computational fluid dynamics and fluid-structure interaction method to the lubrication study of a rotor-bearing system, Tribol. Lett. 38 (2010) 325–336

[16] Q. Lin, Z. Wei, N. Wang, W. Chen, Analysis on the lubrication performances of journal bearing system using computational fluid dynamics and fluid–structure interaction considering thermal influence and cavitation, Tribol. Int. 64 (2013) 8–15

[17] B.S. Shenoy, R.S. Pai, D.S. Rao, R. Pai, Elasto-hydrodynamic lubrication analysis of full 360' journal bearing using CFD and FSI techniques, World J. Model. Simul. 5 (2009) 315–320

[18] E. Kuznetsov, S. Glavatskih, M. Fillon, THD analysis of compliant journal bearings considering liner deformation, Tribol. Int. 44 (2011) 1629–1641

[19] PG. Nikolakopoulos, CA. Papadopoulos, A study of friction in worn misaligned journal bearings under severe hydrodynamic lubrication, Tribol. Int. 41 (2008) 461–472

[20] T. Kazama, Y. Narita, Mixed and fluid film lubrication characteristics of worn journal bearings, Adv. Tribol. 2012 (2012) 1–7

[21] A. Kumar, S.S. Mishra, Steady state analysis of noncircular worn journal bearings in nonlaminar lubrication regimes, Tribol. Int. 29 (1996) 493–498

[22] K.F. Dufrane, J.W. Kannel, T.H. McCloskey, Wear of steam-turbine journal bearings at low operating speeds, J. Lubr. Technol. 105 (1983) 313

[23] H. Hashimoto, S. Wada, K. Nojima, Performance characteristics of worn journal bearings in both laminar and turbulent regimes. Part I: steady-state characteristics, ASLE Trans. 29 (1986) 565–571

[24] P.G. Nikolakopoulos, C.I. Papadopoulos, L. Kaiktsis, Elastohydrodynamic analysis and Pareto optimization of intact, worn and misaligned journal bearings, Meccanica 46 (2010) 577–588

[25] E.R. Nicodemus, S.C. Sharma, Performance characteristics of micropolar lubricated membrane-compensated worn hybrid journal bearings, Tribol. Trans. 55 (2012) 59–70
[26] E.R. Nicodemus, S.C. Sharma, A study of worn hybrid journal bearing system with different recess shapes under turbulent regime, J. Tribol. 132 (2010) 041704
[27] M. Fillon, J. Bouyer, Thermohydrodynamic analysis of a worn plain journal bearing, Tribol. Int. 37 (2004) 129–136
[28] J. Bouyer, M. Fillon, I. Pierre-Danos, Influence of wear on the behavior of a two-lobe hydrodynamic journal bearing subjected to numerous startups and stops. J. Tribol. 129 (2007) 205
[29] W. Litwin, Influence of main design parameters of ship propeller shaft water-lubricated bearings on their properties, Pol. Marit. Res. 17 (2010) 39–45
[30] G.W. Stachowiak, A.W. Batchelor, Engineering tribology, Elsevier Butterworth-Heinemann, 2005

Cite this article as: Y. Wang, Z. Yin, G. Gao, X. Zhang, Analysis of the performance of worn hydrodynamic water-lubricated plain journal bearings considering cavitation and elastic deformation, Mechanics & Industry **18**, 508 (2017)